A low-cost, high-speed, near-infrared hygrometer

A. C. Wilson[a] and T. H. Barnes
Applied Optics Center, Physics Department, University of Auckland, Private Bag 92019, Auckland, New Zealand

P. J. Seakins, T. G. Rolfe, and E. J. Meyer
Fisher and Paykel Healthcare, 25 Carbine Road, Mount Wellington, Auckland, New Zealand

We describe a simple near-infrared hygrometer based on a broadband light-emitting diode (LED) centered at 1320 nm. Light from the LED is collimated and passes through a rotating optical-filter assembly and a sample cell. The water vapor concentration is measured using a synchronous detection scheme. This compact and robust instrument has a response time of 0.15 s and can reliably detect short-term absolute humidity changes as small as 0.6 mg/L (which equate to 0.02% absorption); the long-term stability of the absolute humidity measurement over a period of 4 days is approximately 1 mg/L. These performance characteristics are particularly well suited to measurements associated with human respiration, and we present results in this humidity regime. © *1995 American Institute of Physics.*

I. INTRODUCTION

High-speed, nonintrusive measurement of water vapor concentration is critical to the understanding of many dynamic systems, such as respiratory and combustion systems. Methods based on the dew point can provide an extremely accurate measure of absolute humidity, but the measurement process is slow and dew-point hygrometers can be bulky. Capacitive devices are often compact and low cost, but again the measurement process is slow, and many fail at high water vapor concentrations. The results of numerous investigations of these and other methods of measuring absolute humidity can be found in Ref. 1.

Absorption spectroscopy,[2–5] which offers high speed and high resolution, has been successfully used in a wide variety of gas-sensing applications, including those for water vapor. Near-infrared light-emitting diodes (LEDs) and laser diodes with improved spectral properties have had a beneficial impact on the cost and viability of absorption spectroscopy, but these have been developed primarily for the communications industry, which seeks to *avoid* losses due to absorption by water. Added to the problem of obtaining a near-infrared semiconductor light source with an output wavelength corresponding to regions of "strong" water vapor absorption, the absorption cross section for water vapor is very weak compared to that for other gases, such as carbon dioxide. When low-cost (communications-type) laser diodes near 820 and 1310 nm are used for hygrometry,[6–11] the absorption is very small and the techniques often involve high-speed modulation and frequency stabilization servo-control loops. Stronger absorption and improved resolution are obtained with single longitudinal-mode distributed feedback (DFB) laser diodes near 1390 nm,[12,13] but presently these cost 100 times more than the LEDs we use, and again active frequency stabilization is often required. While a single-mode laser diode can be tuned to the center of a single water absorption line,

the output spectrum of a near-infrared LED has many regions for which water is transparent, so that the theoretical basis for an instrument using such a diode usually involves averaging over many water absorption lines. The integrated absorption observed over the spectral bandwidth for LEDs is generally much less than that for single-mode laser diodes, but—as we shall demonstrate—LEDs can be suitable for absorption spectroscopy of water vapor in the near-infrared-wavelength region where there is a dense population of absorption lines.[14,15]

Blackbody radiation sources such as glow bars[16] or light bulbs can also be used as the infrared light source for spectroscopy applications, but these have several disadvantages. First, obtaining a sufficient spectral density can be difficult. In the near-infrared region, a blackbody source often needs to be hot (>1000 K), and this can cause unwanted heating in a compact instrument. Second, the extremely broadband radiation produced by a blackbody usually requires optical filtering, and this often removes most of the optical power. Also, narrow-bandpass filters sometimes transmit light at wavelengths outside the bandpass region that are still detected. Third, the emitting area of a blackbody source is usually many times larger than that of a semiconductor light source, so that obtaining a uniform and collimated light beam can be difficult. Fourth, if the blackbody radiation source is not contained in a vacuum, heat convection may cause the top of the source to be hotter than the bottom. If a beam is produced with a lens that collects light at a particular point on the blackbody, the spectrum of the light in the beam can change when the source is rotated in the vertical plane. This can limit the allowable orientation of the instrument. Finally, blackbody sources tend to have a slower speed of response than semiconductor devices, and this makes them less suitable for applications where high-speed intensity or frequency modulation is required.

In this paper, we discuss the design and testing of a hygrometer that uses a near-infrared LED and a rotating optical-filter assembly comprising two bandpass filters, one corresponding to a water vapor absorption band and the other

[a] Present address: Clarendon Laboratory, Physics Department, University of Oxford, Parks Road, Oxford OX1 3PU, England.
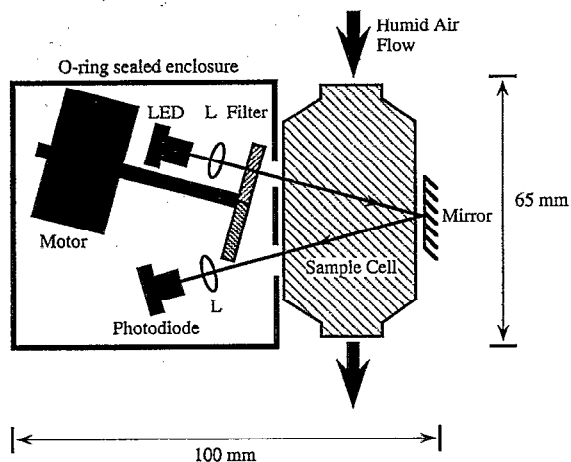
FIG. 1. Schematic of the optical layout.

to a nonabsorbed reference wavelength. This hygrometer provides an accurate, high-speed measurement of water vapor concentration. Light from the LED passes twice through a small sample cell and then is focused onto a germanium photodiode, the output of which is fed to a lock-in detector. This produces an output signal that is approximately linear with absolute humidity. The device is particularly well suited to the humidity range one encounters in respiratory system applications—up to 45 mg/L—where an accuracy of at least ±1 mg/L is important. An excellent introduction to respiratory applications is contained in Ref. 17.

II. DESCRIPTION

A. Optical arrangement

We employ a very simple scheme, depicted in Fig. 1, for the absorption spectroscopy technique. The light source used is an InGaAsP light-emitting diode (Hitachi model HE1301SG), which has an output center-wavelength of 1320 nm and a spectral width of 140 nm. At our typical operating injection current of only 9 mA, the broadband optical-output power is approximately 5 μW.[18] The LED output is collimated with an aspheric lens ($f=6.5$ mm) to form a uniform beam of 5-mm diam. The beam then passes through a dual optical-filter assembly[19] consisting of two semicircular-shaped bandpass filters, each with a transmission of 40%–45% and a bandwidth [full width at half-maximum (FWHM)] of 50±5 nm. One of these filters is centered at 1280±13 nm and the other at 1380±13 nm; the latter corresponds to a dense band of water absorption lines.[20] The light centered at 1280 nm is not absorbed by the water vapor in the sample cell, and is used as a reference intensity in the differential lock-in detector described in Sec. II B. The transmission bands of both filter halves were carefully chosen to avoid absorption bands of other gases that are present in the sample cell. For respiratory applications,[17] the other main gas constituents are carbon dioxide, oxygen, and nitrogen. The circular filter is rotated at 70 Hz using a small, low-noise dc motor (of the type frequently used in portable compact disk players). As shown in Fig. 1, with the aid of a plane aluminum-coated mirror, at a 10° angle of incidence, the

beam makes a simple double pass through a sample cell. The sample cell has plane glass windows, 30 mm apart, making the total beam path length through the water vapor 61 mm. Finally, an aspheric lens ($f=15$ mm) focuses the beam onto a germanium photodiode (Hamamatsu model B1720-02). As the filter assembly rotates, the signal at the photodiode alternates between the absorption and reference wavelengths. The optical power in both absorption and reference signals at the photodiode is 1 μW.

The LED, photodiode, lenses, filter assembly, and motor are all mounted in a rigid o-ring-sealed aluminum enclosure (dimensions are 100×65×40 mm). Before any humidity measurements are made, this enclosure is purged of unwanted atmospheric water vapor in the path of the beam using dry air (water vapor concentration <0.1 mg/L) overnight to remove unwanted water vapor in the path of the beam. An o-ring-sealed window in the enclosure gives the beam access to the sample cell. The instrument is designed to have a removable sample cell that fits into a mounting bracket on the side of the o-ring-sealed enclosure. The plane mirror is permanently mounted in the bracket. If the sample cell is removed, shutters cover the mirror and the o-ring-sealed window so that they are kept clean and undamaged. To avoid unwanted absorption by atmospheric water vapor, the gaps between the o-ring-sealed window, the mirror, and sample cell windows are kept to a minimum: a total of 0.6 mm, in our case. At a room temperature of 298 K, we estimate that this gap introduces a systematic error in the humidity measurement of at most 0.2 mg/L.

A critical element of the hygrometer design is temperature control. Ambient temperature changes affect the spectral characteristics of the LED and the bandpass filters. Thermistors are attached to the LED, filter assembly, and photodiode, and separate proportional integral controllers hold the temperature at the thermistors to 308±0.01 K. Also, the windows of the sample cell are heated (but the temperature is not actively controlled) to 313 K in order to avoid condensation.

B. Light-emitting diode driver electronics and detection scheme

The maximum absorption we obtain with saturated water vapor at 310 K is only 1.8%, and because the LED output intensity is higher at 1280 nm than at 1380 nm, matters are complicated somewhat. However, by modulating the injection current to the LED, we are easily able to measure absorption as low as 0.02% with a standard differential lock-in detection scheme. A block diagram of the LED current driver electronics and the differential lock-in detection scheme is shown in Fig. 2.

The motor that rotates the dual-filter assembly is held at a constant speed (4200 rpm) using a crystal oscillator and a phase-locked loop. An optosensor detects the rotation of the filter, and an error signal is derived by comparing this rotation with a 70-Hz clock signal from the crystal oscillator. This feedback loop locks the phase of the filter rotation to the crystal oscillator to better than 1°.

To obtain the 0.02% resolution with a standard differential lock-in detector, it is critical for the intensity levels of the absorption and reference signals to be identical for dry air in
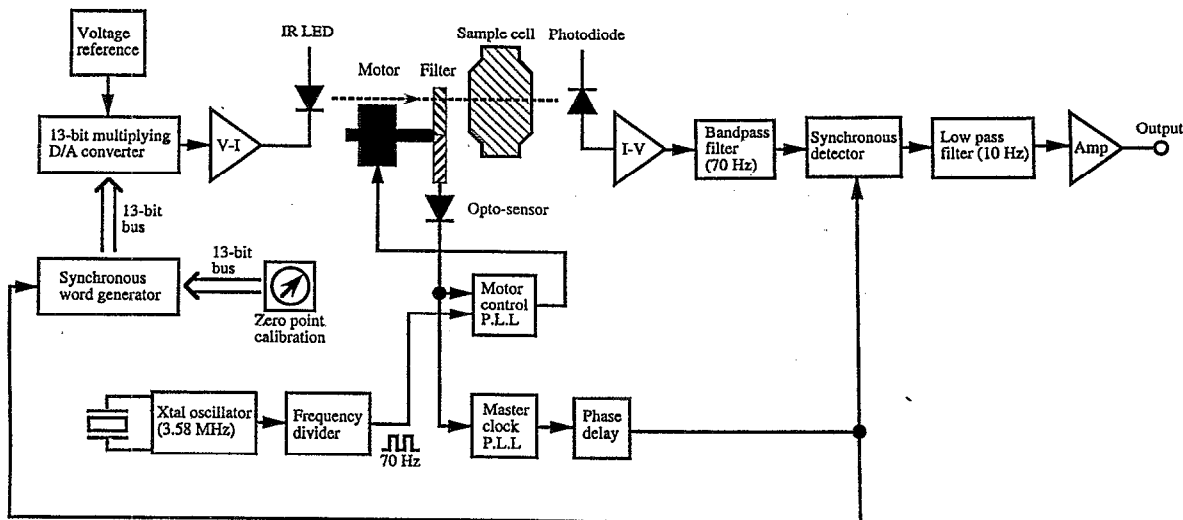
FIG. 2. Block diagram of the LED current driver electronics and the lock-in detection scheme.

the sample cell, because measuring a small absorption signal on top of a comparatively large dc voltage severely limits the dynamic range. However, as mentioned above, the spectral distribution of the LED is not centered between the bandpass wavelengths of the filters; so to balance the intensities, we modulate the injection current to the LED, in a manner that is synchronous with the filter rotation. Since the LED has a spectral peak closer to the reference wavelength, the injection current is attenuated (or reduced) for the half of the filter rotation period corresponding to when the beam passes through the 1280-nm bandpass filter. This process is illustrated in Fig. 3. The amount of current attenuation required also depends on how well the transmissions of the optical-bandpass filters are matched, but in our case this is better than 5%.

To avoid possible problems with the phase locking of the motor (which may be associated with, say, violent movement of the instrument), the clock signal for this synchronous current attenuation (and also for the lock-in detection) is derived from a second phase-locked loop, which takes as its frequency reference the signal from the optosensor used to detect the rotation of the filter. The second (or regenerated) phase-locked loop includes a controllable phase delay, so that the synchronous current attenuation occurs exactly in phase with the rotational position of the correct filter half. To apply the correct amount of synchronous current attenuation, the phase-delayed clock signal is fed to a synchronous word generator, which produces two 13-bit binary words alternately; one corresponds to an *unattenuated* LED intensity, while the other corresponds to an *attenuated* (or reduced) LED intensity. The binary words are generated synchronously with the phase-delayed clock signal, so as to attenuate the LED intensity during the correct part of the filter rotation period. Changing the amount of synchronous current attenuation is achieved with a series of switches (the zero-point calibration control) that change the attenuating binary word. The digital output from the synchronous word generator is then fed to a digital-controlled voltage reference [a 13-bit multiplying digital-to-analog (D/A) converter] which converts

the two different binary words into two different voltage levels corresponding to the two different LED output intensities. Finally, the output from the digital-controlled voltage reference is fed to a voltage-to-current converter, which drives the LED. The net result of all this is that the drive current to the
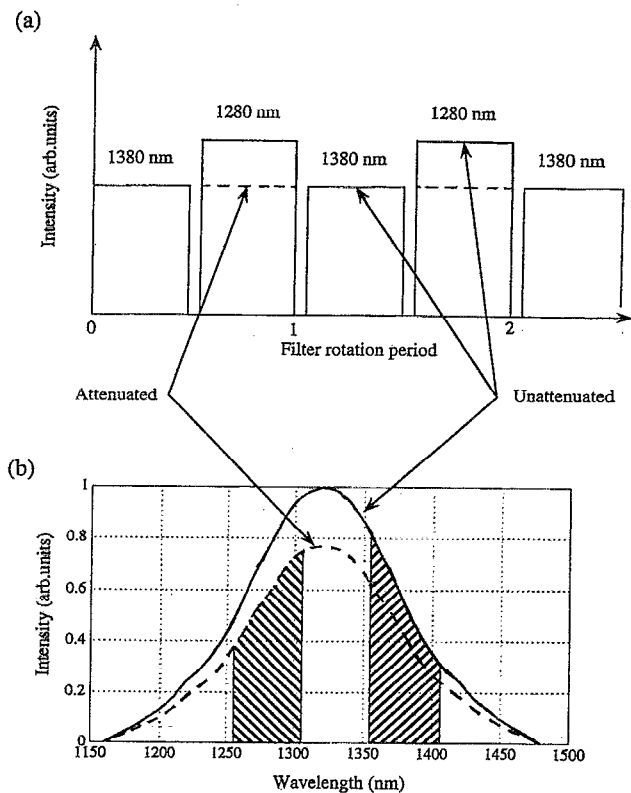

FIG. 3. Sketched illustration of the synchronous attenuation scheme. Without synchronous attenuation, the absorption (1380-nm) and reference (1280-nm) intensities are not balanced, as shown by the solid wave form in (a). Balancing the intensities is achieved by reducing the injection current to the LED when the light passes through the 1280-nm bandpass filter. The spectral output of the LED is shown in (b). Effectively, the synchronous attenuation makes the shaded areas in the two bandpass regions equal.
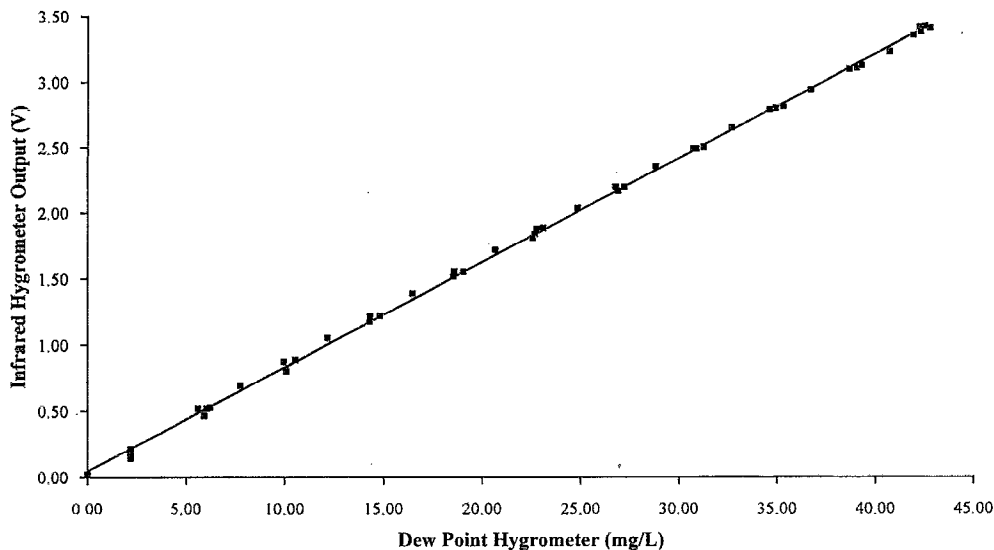
FIG. 4. Calibration with a dew-point hygrometer. Solid line is a linear fit to the data (r=0.9996).

LED switches between two levels, controlled by the synchronous word generator; these levels are thus synchronous with the phase-delayed clock signal.

The zero-humidity point in the calibration of the instrument is set using the zero-point calibration control on the synchronous word generator, so that the differential absorption signal is zero when there is no water vapor in the sample cell. For any fixed value of the digital-controlled reference voltage, the current stability to the LED is better than 1 μA.

Once the absorption and reference intensities have been balanced for zero humidity, the actual detection of absorption by water vapor is relatively straightforward. The germanium-photodiode output is amplified with a low-noise current-to-voltage converter and, together with the phase-delayed clock signal, is fed into a standard lock-in detector (consisting of a bandpass filter, a synchronous detector, a low-pass filter, and an amplifier), the output of which is proportional to the water vapor concentration in the sample cell.

III. RESULTS

We have calibrated the near-infrared hygrometer against a dew-point hygrometer (General Eastern model Hygro-M3) traceable to the National Institute of Standards and Technology. As shown in Fig. 4, the output from the lock-in detector is very nearly proportional to the water vapor concentration in the sample cell. Although we do not expect a linear calibration curve, a straight line with a slope of 12.7±0.1 mg/L per volt fits well to the data points (correlation coefficient r=0.9996). Unfortunately, this result cannot be calculated in a straightforward manner using the Beer–Lambert relation[2] (even in the weak-absorption limit), since the absorption is averaged over many spectral lines. Even with a Beer–Lambert-type relation modified to include the multiple-spectral-line structure of water vapor and the broadband-output spectrum of the LED, calculating the calibration curve is not simple, since water vapor spectral data over our wide wavelength range are complex and not precisely known.[20,21]

To make a conservative estimate of the response time of the near-infrared hygrometer, we used a crude (but effective) valve to switch an 80-L/min air flow through the sample cell from a dry-air source (water vapor concentration <0.1 mg/L) to an air source with a water vapor concentration of 36 mg/L. Time series measurements of the lock-in output were recorded using a computer and a data acquisition card (National Instruments Lab-PC+). From Fig. 5, we obtain a response time (for 0%–90% change) of approximately 0.15 s. This absolute humidity change is typical of those encountered in respiratory systems. We believe that this figure is a conservative estimate, and represents more our inability to produce a faster humidity change in the sample cell than the actual response time of the device. Ultimately, the response time is limited by the low-pass filter to approximately 0.1 s. This can be improved by increasing the cutoff frequency of the low-pass filter, but only at a cost of increased noise.

As well as the fast response time of the hygrometer, we also measured the stability over a period of 4 days using dry air. The dew-point hygrometer was used to check that the absolute humidity remained below 0.1 mg/L over this period. From Fig. 6, we estimate that the long-term stability is approximately 1 mg/L.

We checked that our choice of optical filters eliminates interference from carbon dioxide and oxygen. Changing the gas in the sample cell from dry air to either carbon dioxide or oxygen (both 99.9% pure, and dry) gives an output "error" of +0.3 or +0.1 mg/L, respectively, but these effects are less than the short-term noise of the system. The short-term noise in the hygrometer output is 0.6 mg/L (peak to peak), and originates from ±0.1-Hz changes in the filter rotation frequency, which cause a transient output from the phase-sensitive detector. Other noise sources, such as dark-current noise from the photodiodes and fluctuations in the LED output, do not currently limit the short-term resolution of this device.

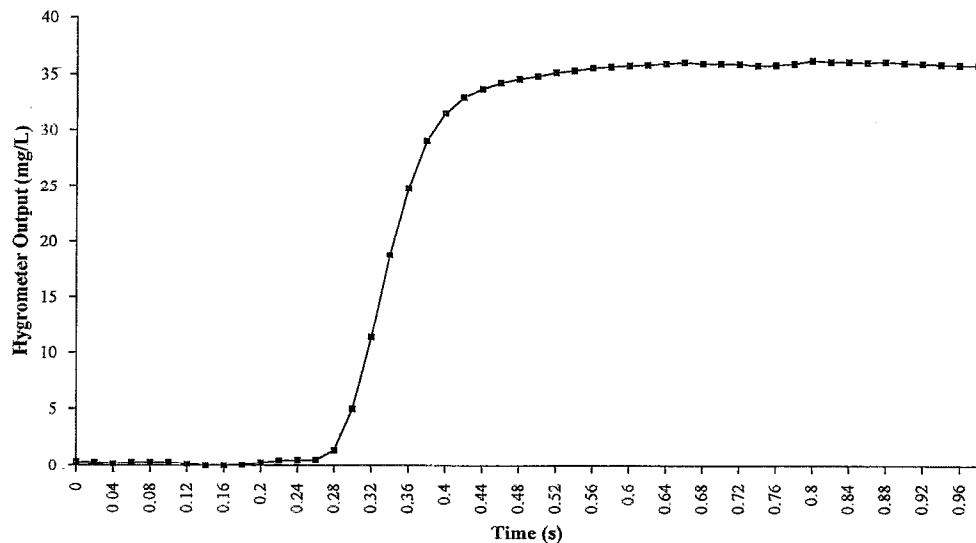As mentioned above, precisely controlling the tempera-

FIG. 5. Response time of the hygrometer.

ture of both the LED and the optical-filter assembly is essential, and failure to do so leads to a calibration that is extremely sensitive to the ambient temperature. Temperature-controlling a filter assembly rotating at 70 Hz is problematic, and best results are obtained when the entire filter assembly is temperature stabilized. We use separate temperature controllers on a shroud around the filter, on the shaft connecting the filter holder to the motor, and on the bearing race supporting the shaft. These hold the temperature of each of these elements stable to better than ±0.01 K; with this attention to detail, the instrument is resilient to ambient temperature changes of ±10 K, as shown in Fig. 7. We observe that a ±10 K change in the ambient temperature, which is large for laboratory and hospital environments, results in an absolute-humidity calibration error of only ∓0.2 mg/L. Also, we calculate that the temperature change used in this mea-

surement results in an air density change that should alter the absolute humidity by only ∓0.01 mg/L, so that when the hygrometer output changes with ambient temperature, this is *not* as a result of a change in the absolute humidity. The sign of this calibration error is consistent with a temperature change of the LED (not the filter assembly), and we are currently investigating this.

If the hygrometer is kept at a constant temperature, but the temperature of dry air passing through the sample cell is changed, we do not observe any change in the hygrometer output. To check the effect of humid-air temperature changes on the hygrometer output, we performed two additional tests. First, when the temperature of the water vapor was varied from 305 to 330 K, but the absolute humidity was held constant (meaning that the water vapor pressure was varied also), we did not observe any change in the hygrometer out-
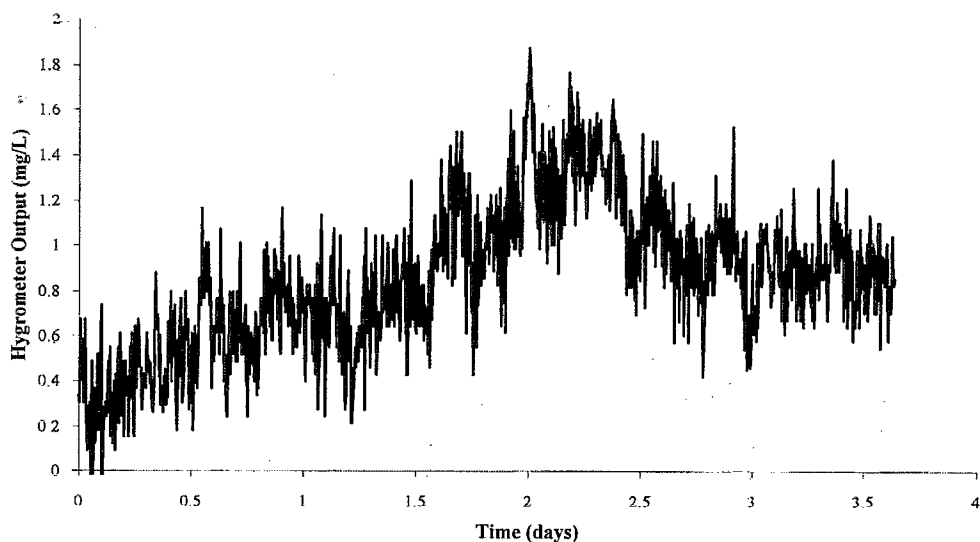

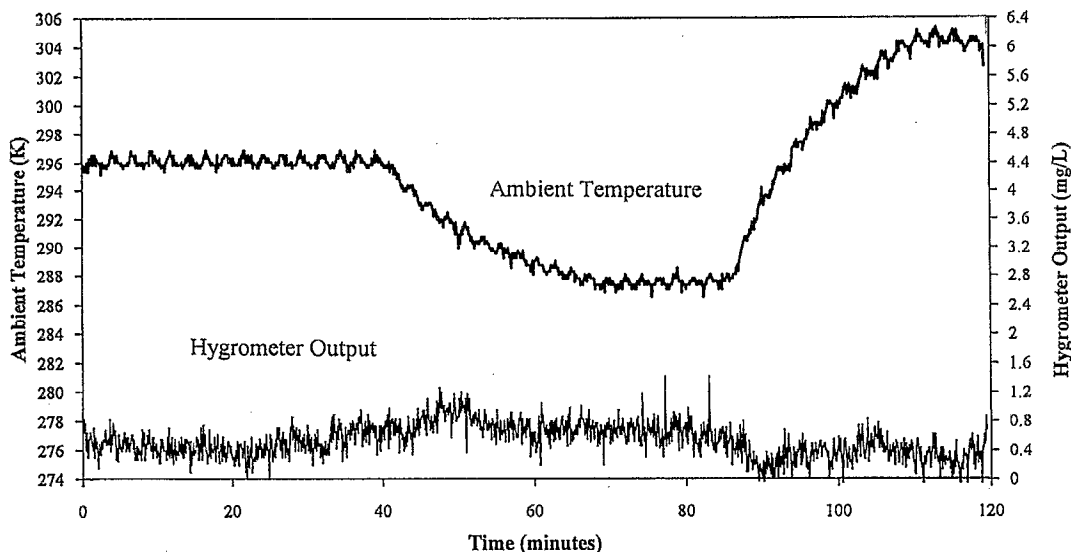FIG. 6. Long-term stability, as measured with dry air.

FIG. 7. Effect of ambient temperature on the hygrometer output.

put. This means that water vapor temperature changes over a range relevant to our application do not alter the hygrometer calibration. Second, when the water vapor pressure was held constant, while the temperature was varied from 305 to 330 K (causing the absolute humidity to change from 25.9 to 24.0 mg/L because of gas expansion), we observed a change in the hygrometer output that corresponds within ± 0.1 mg/L to the change in absolute humidity that one expects from gas expansion. This test confirms that the hygrometer measures absolute humidity. This is what we would expect, because the near-infrared hygrometer measures the number of water molecules present in a volume confined by the infrared beam cross-sectional area and path length in the sample cell. Therefore, by definition, the hygrometer output should be proportional to the absolute humidity of the gas in the sample cell.

IV. DISCUSSION

The instrument described above demonstrates the usefulness of low-cost, near-infrared LEDs for remote sensing of water vapor. Despite its simple design, this system exhibits a quick response and high sensitivity, and its compact configuration eliminates the need to separate the sample cell from the light source and the detector. Combined in a single device, these features are particularly well suited to respiratory system applications, for which conventional hygrometers based on the dew point or capacitive techniques suffer limitations, such as a slow response and failure at high humidity.

Depending on the particular application, there are a number of possibilities for improving the instrument. The absorption path length we use is small so as to keep the instrument compact and the light path simple, but increasing the absorption path length would obviously improve the signal-to-noise ratio. This could be achieved with a multiple-pass sample cell; however, increasing the path length to the optically thick regime might result in a nonlinear calibration curve. If necessary, the injection current to the LED could be increased to compensate for any additional reflection losses

at optical surfaces that result from a more complex sample cell design. The optical output power of the LED is not a limiting factor in this instrument; nevertheless, at high LED injection currents, the self-heating effects can cause shifts in the LED output spectrum.

Precise temperature control of the various components is essential, and at present we use five separate temperature controllers to achieve this. But preliminary measurements indicate that we can sufficiently temperature-stabilize the entire enclosure with a single proportional integral controller and a single thermistor at the LED. This requires more heating power, insulation against environmental temperature changes, and giving careful attention to heat paths within the enclosure.

Splitting in two the broadband collimated beam from the LED and sending the beams through stationary bandpass filters make temperature control of the filters easier, but having different pathways for the absorption and reference beams introduces complications. Contamination on the optical surfaces, including the sample cell windows, is likely to cause far greater calibration problems in a dual-beam configuration than in an arrangement whereby the beams overlap, as in our case. Also, mechanical stability is more critical when the absorption and reference beams have separate pathways.

Failure to completely purge the o-ring-sealed enclosure of residual water vapor results in a small drift with time in the humidity calibration. If purging has not been performed correctly, the calibration drift is most significant immediately after purging has stopped, and drops off in an "exponential-like" fashion over some hours.

Finally, we have made considerable efforts to find a LED with spectral output close to 1380 nm, which would enable us to obtain increased absorption. To the best of our knowledge, such a LED is available only as a customized product, at considerable expense, and in large quantities. We are hopeful that this situation will improve as optoelectronics manufacturers look for applications beyond those in the telecommunications industry.

ACKNOWLEDGMENTS

[1] *Moisture and Humidity, Measurement and Control in Science and Industry* (Instrument Society of America, North Carolina, 1985).

[2] For a discussion of absorption spectroscopy, see W. Demtröder, *Laser Spectroscopy* (Springer, New York, 1981).

[3] D. E. Cooper and R. U. Martinelli, Laser Focus World (November 1992), p. 133.

[4] W. F. Staats, L. W. Foskett, and H. P. Jensen in *Humidity and Moisture, Measurement and Control in Science and Industry*, edited by R. E. Ruskin (Reinhold, New York, 1965), Vol. 1, p. 465.

[5] R. C. Wood, in Ref. 4, p. 492.

[6] D. T. Cassidy, Appl. Opt. **27**, 610 (1988).

[7] L. Wang, H. Riris, C. B. Carlisle, and T. F. Gallagher, Appl. Opt. **27**, 2071.

[8] L. Wang, D. A. Tate, H. Riris, and T. F. Gallagher, J. Opt. Soc. Am. B **6**, 871 (1989).

[9] C. B. Carlisle and D. E. Cooper, Appl. Phys. Lett. **56**, 805 (1990).

[10] N. Goldstein, S. Adler-Golden, J. Lee, and F. Bien, Appl. Opt. **31**, 3409 (1992).

[11] J. A. Silver and D. C. Hovde, Rev. Sci. Instrum. **65**, 1691 (1994).

[12] M. P. Arroyo and R. K. Hanson, Appl. Opt. **32**, 6104 (1993).

[13] M. P. Arroyo, T. P. Birbeck, D. S. Baer, and R. K. Hanson, Opt. Lett. **19**, 1091 (1994).

[14] J. E. Tillman, in Ref. 1, p. 791.

[15] K. Schurer, R. Maandonks, and G. J. W. Visscher, in Ref. 1, p. 775.

[16] D. L. Auble and T. P. Meyers, Boundary Layer Meteorol. **59**, 243 (1992).

[17] S. E. Tilling, A. J. Hancox, and B. Hayes, Clin. Phys. Physiol. Meas. **4**, 197 (1983).

[18] These light-emitting diodes (LEDs) can operate with an injection current as high as 150 mA, at which they produce a broadband output of approximately 22 μW; however, since optical power is not a limiting factor for our application, we use a lower injection current to extend the lifetime of the LED.

[19] The dual-bandpass filter assembly was supplied by Midwest Optical Systems.

[20] L. S. Rothman *et al.*, Appl. Opt. **26**, 4058 (1987).

[21] R. Mücke, B. Scheumann, F. Slemr, and P. Werle, Proc. SPIE **2112**, 87 (1994).